Natural Hazards (2022) 114:2041–2057
https://doi.org/10.1007/s11069-022-05458-w

ORIGINAL PAPER

Tree-ring records of snow-avalanche activity in the Rodna Mountains (Eastern Carpathians, Romania)

Ionela Georgiana Gavrilă[1] · Dariia Kholiavchuk[2] · Iulian Horea Holobâcă[1] · Oles Ridush[2] · Csaba Horváth[1] · Bogdan Ridush[2] · Flaviu Meseşan[1] · Olimpiu Traian Pop[1]

Received: 23 February 2022 / Accepted: 20 June 2022 / Published online: 11 October 2022

Abstract
We reconstruct snow-avalanche (SA) activity along three adjacent avalanche paths in the northern part of the Rodna Mountains (Eastern Carpathians, Romania) using tree-ring analyses. We sampled a total of 238 disturbed Norway spruce (*Picea abies* (L.) Karst.) trees and used the growth anomalies found in tree rings to obtain an avalanche chronology at the subregional scale spanning the 1979–2019 period. Multiple regression analysis of weather data covering the tree-ring-based reconstructed avalanche winters provided three distinct synoptic patterns favoring SA activity: (i) in January, when destabilization of the snow cover occurs during warm periods; (ii) in April, when destabilization of the snow cover is due to the combined effect caused by the warm days and the ones with heavy rainfall; and (iii) in November, during cold periods with snowfalls and strong winds. This study based on the tree-ring approach coupled with multiple regression analysis contributes to a better understanding of the snow-avalanche regime at both local and subregional scale. It also provides the basis for further research to decipher the linkage between the synoptic conditions favoring the naturally released avalanches at a regional scale.

Keywords Snow avalanches · Tree-ring reconstruction · Multiple regression · Rodna Mountains (Eastern Carpathians)

1 Introduction

Snow avalanches (SAs) are widespread natural hazards in high-elevation, temperate and arctic mountain areas worldwide which may threaten residents, tourists, various human activities, destroy the existing infrastructures, and damage the forests. Their formation is related to a complex interaction between terrain, snowpack, and meteorological conditions

✉ Olimpiu Traian Pop
olimpiu.pop@ubbclu.ro

[1] Laboratory of Dendrochronology, Faculty of Geography, Babeş-Bolyai University, 5-7 Clinicilor Street, 400006 Cluj-Napoca-Napoca, Romania

[2] Department of Physical Geography, Geomorphology, and Palaeogeography, Yuriy Fedkovych Chernivtsi National University, str. Kotsyubynsky 2, Chernivtsi 58012, Ukraine

(Schweizer et al. 2003). The frequency of avalanching must be established in recreational mountain areas where there is a stringent need for improving SA hazard mapping. However, the past avalanche activity is often not recorded or even unknown in the remote mountain areas, where the presence of disturbed forests and tree-ring records may fill this gap by providing the possibility to reconstruct past SA activity with annual resolution. An increasing number of studies over the past five decades proved the tree-ring efficiency in detecting past SAs in various mountain areas worldwide from middle to high latitudes: in the Alps (Stoffel et al. 2006; Casteller et al. 2007; Corona et al. 2010; Kogelnig-Mayer et al. 2011; Favillier et al. 2018; Mainieri et al. 2020), Andes (Casteller et al. 2008, 2011), Carpathians (Chiroiu et al. 2015; Gądek et al. 2017; Pop et al. 2016, 2018; Šilhán and Tichavský 2017; Todea et al. 2020), Gaspé Peninsula (Dubé et al. 2004; Germain et al. 2005, 2009), Iceland (Decaulne et al. 2012), Pyrenees (Muntán et al. 2009), Rocky Mountains (Butler and Malanson 1985; Rayback 1998; Reardon et al. 2008; Peitzsch et al. 2021), Scandinavian Mountains (Decaulne et al. 2013, 2014), Sudetes (Tumajer and Treml 2015; Krause and Křížek 2018). Therefore, the frequency and spatial extent of these hazardous phenomenon can be documented using tree-ring analysis in various remote mountain areas lacking historical records, but with field evidence of SA activity attested by disturbed forests. Such areas include the Carpathians too, where SAs are a common forest disturbance driver on the steep slopes in high-mountain areas. Considering the variability of weather conditions across the Carpathian Range (Cheval et al. 2014; Micu et al. 2016), patterns of SA activity may differ in terms of frequency and spatial extent in various parts of these mountains. The SA history in some parts of the Carpathians, e.g., the Southern Carpathians and the Tatras, is relatively known from previous tree-ring reconstructions; however, the Eastern Carpathians remain undocumented. Here, the hazardous phenomenon threatens recreational activities and destroys coniferous forests. The presence of disturbed forests by SAs in this area shows the high potential to reconstruct past SA history from tree-ring analyses. In this study we use tree-ring records to reconstruct SA activity in the northern part of the Rodna Mountains, a high-mountain area in the Eastern Carpathians. Our main objectives are (I) to assess past SA history in three avalanche paths in the northern part of Rodna Mountains and (II) to link the tree-ring reconstructed avalanche winters to synoptic conditions favorable to SA activity.

2 Study area

The Rodna Mountains (Fig. 1) are the highest part of Eastern Carpathians (Romania), reaching a maximum altitude of 2303 m above sea level (a.s.l.) (Pietrosul Peak), high enough to support the formation of small glaciers during cold intervals of the Late Pleistocene. The Rodna Mountains, along with Maramureş and Călimani Mountains, were the second center of the Pleistocene glaciations in the Romanian Carpathians. Their overall glacial morphology is represented by arrow crests, pyramidal peaks, glacial cirques, and U-shaped valleys shaped by the numerous former glaciers (Mîndrescu et al. 2010). They result from the Pleistocene glaciations which extended from the highest peaks to below 1400 m a.s.l. (Urdea and Reuther 2009). The present-day geomorphic processes, including SAs, reshape the steep slopes resulted from glacial erosion. We performed dendrogeomorphic investigations within three distinct channeled avalanche paths in the northern part of Rodna Mountains, on the left side of Buhăescu valley, one of the glacial valleys descending from the main crest in the high-mountain area. The avalanche terrain investigated is on the

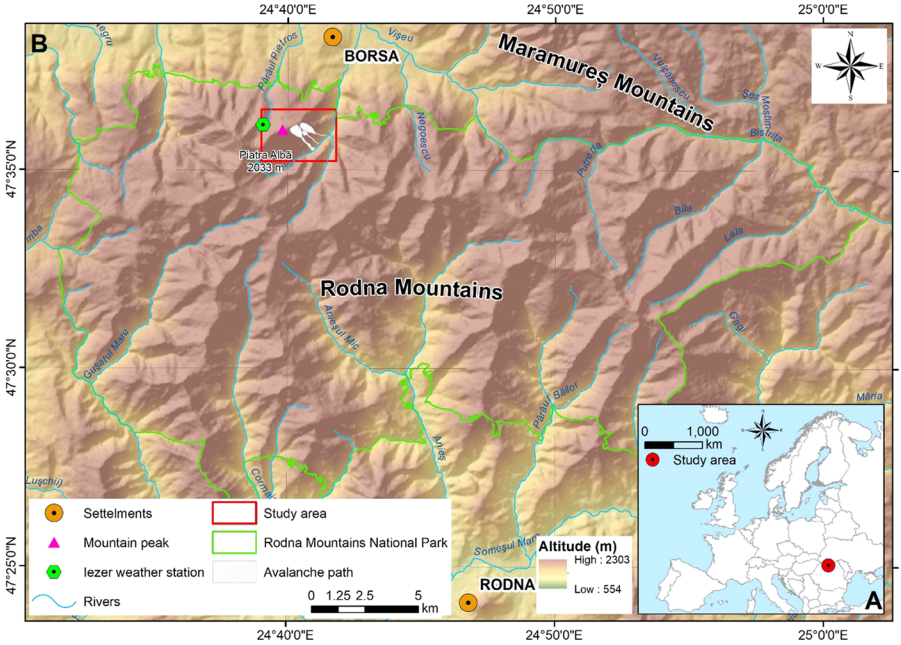

Fig. 1 Map showing the location of the Rodna Mountains in Romania (red circle in Fig. 1A) and zoom in the investigated avalanche paths location (Fig. 1B)

Buhăescu valley slopes below Piatra Albă Peak (2034 m a.s.l). We located the avalanche paths on the steep slopes between 1850 m a.s.l in the starting zones and 1020 m a.s.l. in their runout zones. The slope declivity ranges between 35–45° and > 45° in the starting zones, whereas in the runout zones, at the confluence with Buhăescu valley, the slope angle decreases below 25°. Usually, the avalanches stop on the opposite side slope of the valley, as evidenced by disturbed forest here.

The Rodna Mountains have a moderate continental climate with North-Atlantic influences. The mean annual temperature varies between 0 and 2 °C in the runout areas of the paths, and −2… 0 °C at altitudes above 2000 m a.s.l, as indicated by the instrumental records (1961–2007 period) at the Iezer Weather Station (1785 m a.s.l.) located on the adjacent valley in the western part of the study area. The mean multi-annual precipitation is 1250 mm and the mean multi-annual snowpack thickness is 55 cm, with the highest values recorded in 1961 and 1995. The winter season is characterized by negative average temperatures allowing for snowpack of variable depths to form (Fig. 2). For example, on northern facing slopes, snow may last all year round, but they could also last only until the end of summer (Dragotă and Kuksicsa 2011); hence, a permanent snowpack is missing. The vegetation cover is developed in typical altitudinal belts. In the starting area of the avalanche paths, alpine meadows, bare rock surfaces, and discontinuous shrub patches of *Pinus mugo* and *Juniperus communis* are present. Downslope along the track and the runout zones of the paths, the vegetation consists of coniferous forests dominated by the Norway spruce (*Picea abies* (L.) Karst.) and mixed coniferous-broadleaves forests with European beech (*Fagus sylvatica*). The paths investigated are situated within the Rodna Mountains National Park (the second oldest national park in Romania), as a protected area where human intervention is not allowed, except for tourism activities. Therefore, any

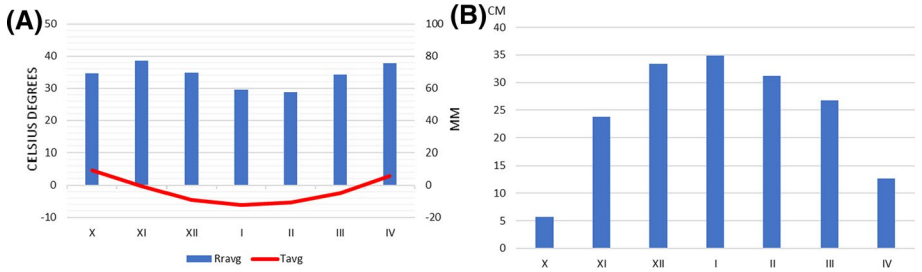

Fig. 2 Ombrothermic diagram (**A**) and snow thickness variability during winter season (**B**) at Iezer weather station (1961–2010)

possible anthropogenic disturbances on forest stands that may bias the dendrogeomorphic reconstruction are excluded.

3 Data and methods

3.1 Field mapping and tree sampling

We conducted two field campaigns in summer and autumn of 2019 when we chose three avalanche paths (path 1—P1; path 2—P2; and path 3—P3 hereafter) located in the Buhăescu left valley-side slopes (Fig. 3) for tree-ring investigations. We made this selection taking into consideration how representative these paths are for SA hazard assessment, their location in the proximity of the weather station, the presence of tourism infrastructure (hiking trails) in their runout zones, and their accessibility. We then draw sketch maps with a preliminary delineation of the spatial extent of the paths on orthophotoplans using clearly defined trimming patterns of forest vegetation attributed to past SA activity. Selected study sites were then identified in the field, and the avalanche path borders as recognized by the spatial extent of disturbed trees due to recent avalanche activity were corrected on the sketch maps. We focus on tree sampling sites in the runout and track zones of the paths where the high-magnitude SAs are expected to be large enough to reach these areas. After a field inspection of trees living throughout the three avalanche paths, we identified and selected disturbed Norway spruce (*Picea abies* (L.) Karst.) trees. We systematically sampled only trees showing clear evidence of external damages, namely scarred, uprooted and/or tilted stems, apex loss, stripped branches, which are likely to result from SA impact (Burrows and Burrows 1976; Stoffel et al. 2013), regardless the position of damages on the stems, tree height, and circumference. Using a GPS device, we determined their spatial position within the avalanche path and integrated the point coordinates into a GIS database. We carefully selected the trees, by discarding those growing near the river or those located in the proximity of the forest road crossing the runout zone, which could possibly bias our SA reconstruction since they could be disturbed by other processes like hydrogeomorphic or human activities.

Depending on the diameter, height, and position of damages on stems, we extracted 2, 3, or 4 cores per tree using Pressler borers of variable lengths (40–80 cm). In the case of wounded trees, we took at least two cores per tree: one crossing the scar, another from the opposite side of the stem, and an additional one, next to the scar. This sampling approach

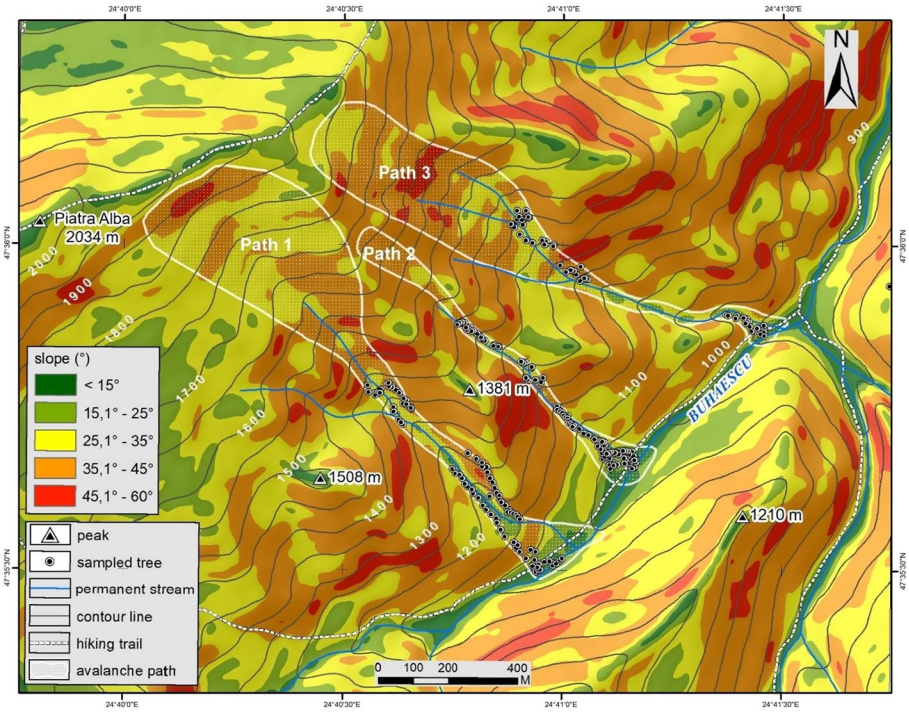

Fig. 3 Slope map of the avalanche terrain and the location of trees sampled within the three paths investigated

allows us to detect the tangential rows of traumatic resin ducts, representing a typical growth reaction of *Picea ssp*. (Stoffel 2008) due to mechanical impact caused by SAs. We sampled tilted trees at variable height on the stem, in the place of maximum stem tilting, and topped trees below the broken stem, at a level where the cambium is still active. We also sampled wounded, tilted, topped, and partially uprooted but still in situ living trees using a chainsaw. Hence, our collection includes cores and discs from a total of 238 disturbed trees: 93 along P1 (166 cores from 67 trees and one stem disc per tree from 26 trees), 92 along -P2 (132 cores from 66 trees and one stem disc per tree from 26 trees), and 53 along P3 (54 cores from 27 trees and one stem disc per tree from 26 trees). The tree species, social position of individuals, nature of visible damages on stems, measurement of height and stem circumference at breast height, side, and height of sampling on the stem, as well as photographs of each sampled tree have also been collected in the field. In order to build a local reference chronology, we also sampled a set of undisturbed trees (42 cores from 22 trees) growing outside of the paths.

3.2 Tree-ring analyses

We performed ring-width measurements and anatomical analyses on all of our samples (cores and discs) following dendrochronological procedures described in Bräker (2002); Stoffel and Bollschweiler (2008); Stoffel and Corona (2014). Sample preparation includes core mounting on wood supports, air-drying, and sanding of samples using a sanding belt

machine with sanding belts of progressively finer grits (80, 180, 220, 400, 600) until the wood sample surfaces revealed the ring boundaries and their anatomical structure. We then determined the tree age by ring counting and measured the ring width to the nearest of 0.01 mm accuracy using a LINTAB 5 system composed of LEICA DMS 1000 stereomicroscope coupled with a measurement table connected to a computer with TSAPWin™ Scientific software (RINNTECH 2021). To identify the trees' growth anomalies caused by SA activity, we performed macroscopic analyses on samples from disturbed trees. We also identified typical growth disturbances (GDs) within rings caused by the mechanical impact of SAs (Stoffel and Corona 2014), such as impact scars (SC), traumatic resin ducts (TRD), and compression wood (CW) in association with abrupt onset of growth suppression (GS) sequences. Growth reactions developed in the first decade in the rings of disturbed trees were not taken into consideration, as during this period, the young trees may be damaged by various disturbances other than SAs and, therefore, represent a potential source of dating errors for SA chronologies (Šilhán and Stoffel 2015; Tichavský et al. 2017). To obtain the local reference chronology, to crossdate it with the ring-width series from disturbed trees and to differentiate between growth anomalies caused by SAs and the normal growth of trees under the climatic conditions (Bryant et al. 1989), we measured tree-ring growth series from trees located outside the paths in undisturbed sites by SAs. Thus, we visually and statistically crossdated our reference chronology against the growth chronologies of each disturbed tree using COFECHA software (Holmes 1983) for two reasons: (i) to detect possible false or missing rings and correct ring-width series of disturbed trees and (ii) to discriminate between growth anomalies found in disturbed trees which are related to SA activity and the growth of the trees influenced by the climatic factors.

3.3 Event determination, avalanche activity index, and return period reconstruction

We classified the growth reactions into three intensity classes (strong, moderate, and weak) based on the criteria described by Stoffel and Corona (2014). The number and type of growth disturbances found within rings served to calculate an avalanche activity index (AAI, %) expressed as a ratio between the number of disturbed trees in a particular year and the total number of trees alive in that year (Shroder 1978; Germain et al. 2009), as follows:

$$\mathrm{AAI}_t = \left(\sum_{i=1}^{n} \mathrm{R}_t\right) / \left(\sum_{i=1}^{n} \mathrm{A}_t\right) \times 100$$

where (R) represents the number of trees showing strong and moderate GDs in a particular year (t); (A) indicates the total number of sampled trees alive in the particular year (t). To define a specific SA winter, we assumed that the following cumulative criteria must be met: (i) a minimum of 3 disturbed trees out of ten trees alive in a particular year must show GDs of strong and moderate intensities in their growth rings; and (ii) an avalanche activity index (AAI) $\geq 10\%$. Based on the tree-ring reconstructed avalanche winters, we calculated the return periods considered as the average period within which the SAs reach a given location in the path (McClung and Schaerer 2006) for each path investigated. We also calculated the Regional Avalanche Activity Index (RAAI, %), as proposed by Germain et al. (2009) using the following formula:

$$\mathrm{RAAI}_t = \left(\sum_{i=1}^{n} \mathrm{AAI}_t\right) / \left(\sum_{i=1}^{n} \mathrm{P}_t\right)$$

where AAI represents the avalanche activity index for a specific avalanche path in the year (t) and (P) is the number of paths recording an avalanche in the year (t). To reduce the influence of local factors on avalanche activity and to identify those winter seasons when climatic conditions favor the SA activity at sub-regional scale, we considered only years with reconstructed SA winters in the investigated paths for our RAAI calculation, as suggested by Germain et al. (2009).

3.4 Meteorological data analysis

We analyzed the daily climatic data (temperature, precipitation, wind, and snow cover) recorded at the Iezer meteorological station (1785 m a.s.l., 47°36′ N, 24°39′ E,) over the time period between 1961 and 2015 (Tank et al. 2002). For each climatic variable, we considered several parameters (Table 1) including the average and extreme values for each parameter during the snow cover season (November–April), as shown in Table 2.

3.5 Multiple regression analysis

We chose a regional approach of the SA activity. In the multiple regression analysis, instead of considering the avalanche winters reconstructed by using the AAI calculated for each avalanche path, we calculated the RAAI to reconstruct avalanche winters in the three paths, and we used this index as dependent variable. Thus, we obtained the highest scores for those years when such events occurred on all three avalanche paths and when the role of weather factors was dominant in preparing the conditions for the onset of avalanches. Using multiple regression, we correlated the RAAI with 50 monthly climate variables (1961–2015) that we chose empirically based on the weather parameters recorded at the Iezer weather station. The multiple regression also allowed us to determine the model's overall fit (explained variance) and the relative contribution of each of the predictors to the total explained variance. We used the stepwise method with the SPSS software to calculate the regression parameters, and we considered a 95% confidence level to keep climate variables significantly contributing to the total variance.

4 Results

4.1 Tree-ring reconstructed events

The cores and discs from 238 disturbed trees sampled in all avalanche paths allowed us to identify 1035 growth anomalies of strong and moderate intensities, from which 110 SC (10,62%), 423 TRD (40,86%), 301 GS (29,08%), and 201 CW (19,42%). Using the distribution of these tree-growth anomalies, we reconstructed the avalanche years in each investigated path. Table 3 and Fig. 4 shows the three paths' tree-ring reconstructed avalanche winters. We identified 14 avalanche years in P1 and P2 spanning the most extended period with SA records (1970–2019) and only 12 in P3 covering the 1978–2019 period. The return periods values range between 3.5 in P1 and P2 and 3.4 years in the P3. The RAAI

Table 1 The climatic variables and parameters examined in the multiple regression analysis

Air temperature	
Tavg	Average temperature
Tmin	Minimum temperature
Tmax	Maximum temperature
N_Tmin < 1STD	Number of days with minimum temperature below monthly average minimum temperature minus one standard deviation
N_Tmin < 2STD	Number of days with minimum temperature below monthly average minimum temperature minus two standard deviations
N_Tavg > 1STD	Number of days with average temperature above monthly average temperature plus one standard deviations
N_Tavg > 2STD	Number of days with average temperature above monthly average temperature plus two standard deviations
N_Tmax > 1STD	Number of days with average temperature above monthly average temperature plus two standard deviations
N_Tmax > 1STD	Number of days with maximum temperature above monthly average maximum temperature plus one standard deviations
N_Tmax > 2STD	Number of days with maximum temperature above monthly average maximum temperature plus two standard deviations
N_tavg > 0 °C	Number of days with average temperature above freezing point
N_tavg > 0 °C_SC > 5 cm	Number of days with average temperature above freezing point with snow thicknesses above 5 cm
Wind	
Vavg	Average wind speed
Vmax	Maximum wind speed
N_Vavg > 1STD	Number of days with average temperature above monthly average temperature plus one standard deviations
N_Vavg > 2STD	Number of days with average temperature above monthly average temperature plus two standard deviations
Precipitation	
RR	Monthly sum of precipitation
N_RR > 1STD	Number of days with daily sum of precipitation above daily average sum of precipitation plus one standard deviations
RR_SC	Sum of precipitation for the days with snow cover
RRmax24h	Maximum precipitation amount in 24 h
RRmax72h	Maximum precipitation amount in 72 h
Snow thicknesses	
ST_max24h	Maximum snow thicknesses in 24 h
ST_max72h	Maximum snow thicknesses in 72 h
ST_month	Snow thicknesses accumulated during a month
N_STUP_1_10cm_24h	Number of days with increasing snow thickness from 1 to 10 cm in 24 h
N_ST_UP_10_15cm_24h	Number of days with increasing snow thickness from 10 to 15 cm in 24 h
N_ST_UP_15_20cm_24h	Number of days with increasing snow thickness from 15 to 20 cm in 24 h
N_ST_UP_20_25cm_24h	Number of days with increasing snow thickness from 20 to 25 cm in 24 h
N_ST_UP > 25cm_24h	Number of days with increasing snow thickness greater than 25 cm in 24 h
N_ST_UP_1_25cm_72h	Number of days with increasing snow thickness from 1 to 25 cm in 72 h
N_ST_UP_25_50cm_72h	Number of days with increasing snow thickness from 25 to 50 cm in 72 h
N_ST_UP > 50cm_72h	Number of days with increasing snow thickness greater than 50 cm in 72 h
N_ST_UP	Number of days with increasing snow thickness

Table 1 (continued)

N_UP_ST_ > 1STD	Number of days with increasing snow thickness greater than one standard deviation
N_UP_ST > UP_avg_	Number of days with increasing snow thickness greater than average snow thickness increase
N_ST < 10 cm	Number of days with snow thickness less than 10 cm
N_ST_10_20cm	Number of days with snow thickness from 10 to 20 cm
N_ST_20_30cm	Number of days with snow thickness from 20 to 30 cm
N_ST_30_40cm	Number of days with snow thickness from 30 to 40 cm
N_ST_40_50cm	Number of days with snow thickness from 40 to 50 cm
N_ST_50_60cm	Number of days with snow thickness from 50 to 60 cm
N_ST > 60 cm	Number of days with snow thickness greater than 60 cm

Table 2 The climatic variables and parameters analyzed

Air temperature			
Tmed	Tmin	Tmax	N_Tmin < 1STD
N_Tmin < 2STD	N_Tavg > 1STD	N_Tavg > 2STD	N_Tmax > 1STD
N_Tmax > 2STD	N_tavg > 0o C	N_tavg > 0 oC _SC > 5 cm	
Wind			
Vavg	Vmax	N_Vavg > 1STD	
Precipitation			
RR	N_RR > 1STD	N_RR > 2STD	RRravg_SC
RRmax24h	RRmax72h		
Snow Cover			
Nmax24h	Nmax72h	LT_I	UP_10cm_24h
UP_10_15cm_24h	UP_15_20cm_24h	UP_20_25cm_24h	UP_ > 25cm_24h
UP_25cm_72h	UP_25_50cm_72h	UP_ > 50cm_72h	N_UP_SC
N_UP_SC_ > 1STD	N_UP_SC > UP_avg_	N_SC < 10 cm	N_SC10_20cm
N_SC20_30cm	N_SC30_40cm	N_SC40_50cm	N_SC50_60cm
N_SC > 60 cm			

Abbreviations in the table indicate: T, temperature; V, wind speed; RR, precipitation; SC, snow cover; min, minimum; max, maximum; avg, average; LT, layer thickness; N, number of days; UP, growth; STD, standard deviation

(%) calculated using the AAI (%) of reconstructed years in each path revealed in total nine distinct years in which SA activity affected the three paths investigated. The RAAI (%) values range between 19.8 and 33% (Table 4), exceeding the threshold values (10%) proposed by previous studies (Germain et al. 2009).

4.2 Regression analysis

The regression analysis provided eighth models of synoptic conditions favorable for SA activity. We selected the models that explain more than 80% of the total variation (Table 5) obtained from multiple regression analysis.

Table 3 Number, type, and intensities of growth anomalies (SC, scars; TRD, traumatic resin ducts; GS, growth suppression; CW, compression wood; *s*, strong, and *m*, moderate intensities) found in disturbed trees and the AAI (%) calculated for the reconstructed event years in each path

Years	Sample depth	Disturbed trees	Growth anomalies							AAI (%)
			SC	TRD		GS		CW		
				s	m	s	m	s	m	
Path 1										
2015	93	23	2	8	11		2		2	24,7
2012	93	25	2	5	10		25		2	26,8
2009	93	17	6	9	16		11		5	18,2
2006	93	22	2	3	15	1	3	2	3	23,6
2005	92	26	7	9	10		6	1	1	28,2
2002	91	15	2	8	9		5	2	3	16,4
2000	91	55	8	21	14	3	16	14	15	60,4
1995	87	39	6	10	11		22	2	3	44,8
1989	78	10	1	1	2	1	5		4	12,8
1985	71	17	2	7	2		4	1	2	23,9
1981	62	20		3	7	1	11		2	32,2
1978	53	23	7		13		6		2	43,3
1974	39	12	5		5		8		3	30,7
1970	28	7	1		4		3		2	25
Path 2										
2015	92	13	4	4	4		5		1	14,1
2012	92	19	1	5	5		14		3	20,6
2009	92	21	4	11	3		7		9	22,8
2006	92	25	5	7	6		8	1	14	27,1
2005	92	14	3	5	3	1	7	1	5	15,2
2002	86	40	6	12	9	1	16		14	46,5
1999	84	40	3	10	11	1	20	3	16	47,6
1995	78	19	1	2	3	1	9	1	6	24,3
1991	68	8			4		3		2	11,7
1989	64	11	1	2	2		5		3	17,1
1985	58	16	2	5	5		6	1	3	27,5
1981	52	10	2	6			5		1	19,2
1978	48	8		1	2	1	4		1	16,6
1970	35	6			2	2	2		2	17,1
Path 3										
2015	53	11	3	3	2				5	20,7
2012	53	17	5	9	1	1	7	2	10	32
2009	53	10	3	4	4		3		2	18,8
2006	52	21	5	7	5		8		7	40,3
2005	51	10	3	4	4		4	1	3	19,6
2002	49	18	2	5	3		12	2	4	36,1
1999	41	22	4	4	7		6	2	10	53,6
1995	37	14	2	6	3		9		5	37,8
1991	34	6		2	1		1	1	1	17,6

Table 3 (continued)

Years	Sample depth	Disturbed trees	Growth anomalies						AAI (%)
			SC	TRD		GS		CW	
				s	m	s	m	s	m	
1989	33	4			1		3		1	12,1
1985	30	7			1		2	1	5	23,3
1978	21	6	1	4	1		4	1	2	28,5

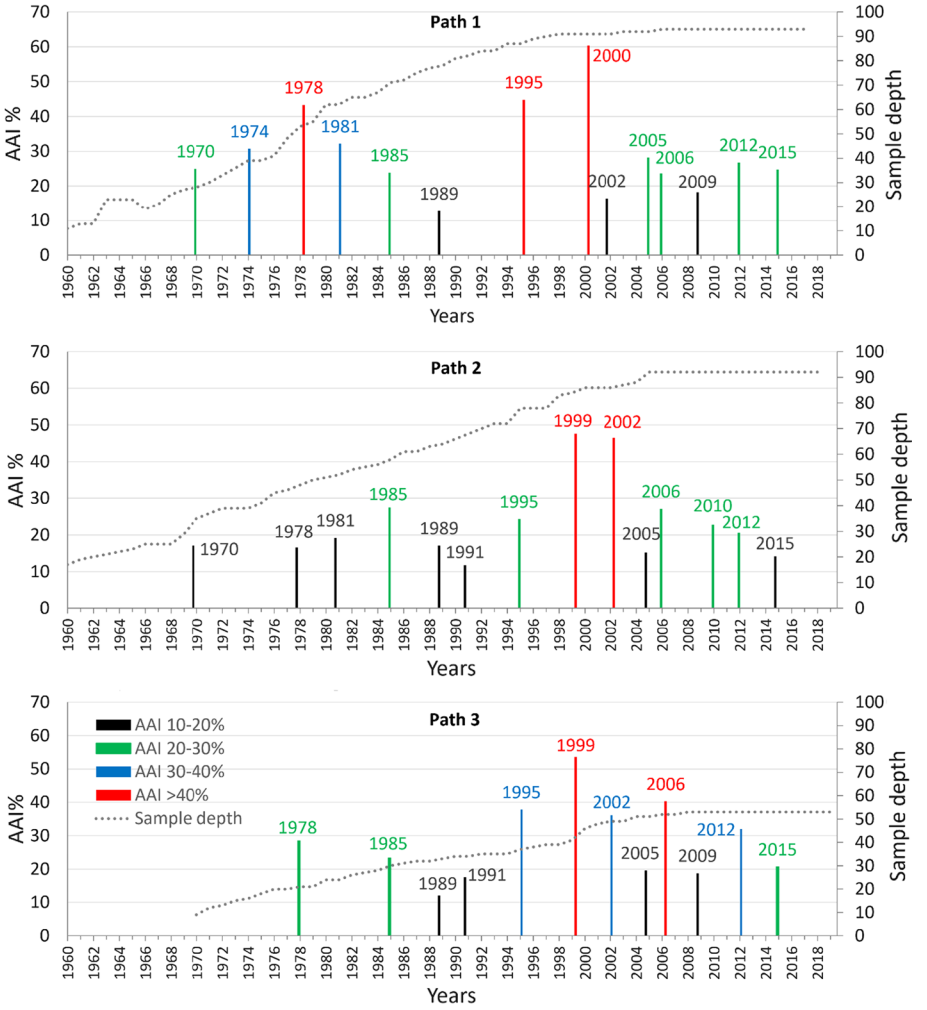

Fig. 4 Event-response histograms indicating the reconstructed avalanche winters in the investigated avalanche paths

Table 4 Regional Avalanche Activity Index (RAAI, %)

Years	RAAI (%)
2015	19.8
2012	26.4
2009	19.9
2006	30.3
2005	21
2002	33
1995	35.6
1985	21.2
1978	25.7

Table 5 Regression analysis summary

R	*R* square	Adjusted *R* square	STD error of the estimate
9.14	0.835	0.803	0.115

Table 6 Regression coefficients for climate variables

Model	Unstandardized coefficients		Standardized coefficients (beta)
	B	Standard error	
Intercept	− 0.546	0.103	
N_Tavg > 2STD_ian	0.487	0.049	0.683
N_ST > 60cm_ian	0.009	0.001	0.441
N_SCUP_15_20cm_24h_ian	0.352	0.073	0.325
N_RR > 2STD_apr	0.146	0.024	0.405
N_Tavg > 2STD_apr	0.106	0.033	0.226
RRmax72h_apr	0-.008	0.002	-0.315
N_Tmin < 1STD_oct	0.082	0.012	0.446
N_Vavg > 1STD_nov	0.026	0.005	0.363

We identified the scenarios for the occurrence of the avalanche events based on the variables retained by the regression (Table 6). The influence of each variable in the total variation suggested by the standardized beta coefficients helped us prioritize the climatic factors.

The results indicate the favorable climatic factors for two avalanching periods in the middle to late winter season and a period corresponding to the beginning of the avalanche season:

(i) In January, the number of very hot days (Tavg > 2 * SD) influences the stability of the snow layer. For the same month, the presence of a thick snow layer (the number of days when the SNC height exceeds 60 cm) and its rapid growth (the number of days with an increase of 15–20 cm in 24 h) are essential for avalanche activity;

(ii) In April, when usually melting avalanches are dominant, the snow cover becomes unstable due to the presence of days with heavy rainfall (RR > 2 * STD) and very high temperatures;
(iii) At the beginning of the avalanche season, the role of low temperature (tmin < 1*STD) in October which would allow the early formation of the snow cover is noticeable, but also the high wind speeds in November (Vavg > 1*STD), which favor the relocation of snow.

5 Discussion

In this study, we obtained a chronology of avalanche activity at the subregional scale for the northern part of Rodna Mountains using tree-ring records. Our analysis covers roughly the last four decades (1979–2019). We identified nine SA winters in all three investigated paths, through RAAI calculation. In the absence of historical records of avalanche occurrences, the tree-ring reconstruction remains the unique source of information regarding the SA activity for this mountainous region in Eastern Carpathians. As this tree-ring chronology from Rodna Mountains is the first of this kind in the Eastern Carpathians, it will represent a starting point in the comparative analysis of SAs in other paths in this mountain area. Similar chronologies at the subregional scale should be extended in other paths of the Rodna Mountains, in order to allow comparisons between them and to have the possibility to decipher the avalanche regime at a regional scale.

The SA winters reconstructed in the three paths investigated allowed us to calculate an average return interval of 4.4 years for the time period 1979–2019. This value is higher than the average return interval calculated for each path of 3.5 and 3.4 years in P1 and P2, and in P3, respectively. This slight difference may be attributed to each path's different sample depth and the length of the reconstructed periods. For example, in P3, a smaller sample depth and a shorter period covered provided only 12 reconstructed SA winters, compared to P1 and P2, where higher sample depth and longer periods covered provided 14 reconstructed SA winters. The return interval varies also within the three avalanche paths; this may suggest that other factors than the weather conditions may favor snow avalanching and tree-ring reconstruction of avalanche winters. Also, a complex interaction of local factors, such as the slope, aspect and associated snow drifting, snow metamorphism (Schweizer et al. 2003), tree-age structure, tree density, species and size, growth anomalies type (Šilhán et al. 2019; Tichavský and Šilhán 2016) may influence the reconstructed SA pattern at the path scale. Investigating all these interactions between the local factors favoring SAs, as well as the ability of trees depending their characteristics to record past SA activity, represents challenging issues and needs to be addressed in further studies of similar geoecological context.

The number of avalanches and the time interval reconstructed is limited because the high-magnitude or more recent avalanche events may have uprooted and destroyed trees reducing the available records. Hence, estimating changes in the avalanche regime attributed to a climatic trend from the tree-ring-based reconstructed period is challenging. As a consequence, we did not identify any trends in the SA pattern and frequencies for longer periods than the last four decades in our reconstructed SA history due to the limited records.

In the present study, the tree-ring SA events reconstructed in each individual path resulted by applying a cutoff values of the AAI ≥ 10%, as well as the minimum 3 sampled

trees showing growth reactions of strong and medium intensities sensu Stoffel and Corona (2014). The AAI (%) values applied by various authors in their studies are strongly dependent on sample size, ranging between 40%, in the case of a small sampling size (Butler and Malanson 1985; Butler and Sawyer, 2008; Muntán et al., 2009), and 10% in the case of higher sampling size (Boucher et al., 2003; Dubé et al., 2004; Germain et al. 2005, 2009; Reardon et al., 2008). For the present study, the high sampling size and sample type (including more than 20 cross-sections sampled in each path) allowed us to adopt an AAI ≥ 10% to define SA events. As in the present study in Rodna Mountains none of the events reconstructed by tree rings were confirmed by historical archives. Here we adopted these cutoff values of AAI considering that these minimum AAI (%) values are appropriate to reconstruct past events, as proven by studies using these AAI (%) values in other paths from Southern Carpathians (Pop et al., 2016, 2018) where few tree-ring reconstructed events were also confirmed by historical records.

Previous studies on reconstructing SA chronologies in other mountain avalanche-prone area reported fluctuations in the trends of natural SA activity, indicating either an increase (Butler and Malanson 1985; Germain et al. 2009) or a decrease (Giacona et al. 2021) of SA activity. One of the major limitations of tree-ring methods is that even though multiple SA events potentially occur during the same winter season, only a single event may be reconstructed and attributed to this winter season. Therefore, SA frequencies inferred from tree rings should be regarded as minimum frequencies reconstructed.

According to projected climate variability in Rodna Mountains, the thick snow cover, usually specific in December–January period, is expected to shift to March–April period (Dragotă and Kucsicsa 2011). Consequently, SA activity in the study area may potentially increase in the late winter season, given the high number of days with temperature above 0 °C, specific for this period of winter season.

The tree-ring-based reconstructed avalanche winters can further be used to identify the synoptic controls on avalanche activity and to inform hazard management decision-makers regarding the past frequency and spatial extent of SAs in the affected areas. From the perspective of the applicability of the research findings presented in study, our reconstructions may be useful for the managers of the protected areas, particularly for the Administration of the Rodna Mountains National Park, in their efforts to mitigate the SA hazard and to implement adequate avalanche hazard planning and tourism activities.

6 Conclusion

We derived an avalanche chronology from tree-ring records in the northern part of the Rodna Mountains, a subregion of this mountain range where historical archives of SA activity are lacking. By analyzing samples from 238 disturbed trees growing within three avalanche paths, we reconstructed 14 avalanche winters in P1 and P2 between 1970 and 2019, and 12 avalanche winters in P3 covering the period 1979–2019, with an averaged return periods of 3.5 years in P1 and P2, and 3.4 years in P3.

The analysis of weather conditions during the nine winter seasons when avalanches occurred in all three paths investigated revealed three distinct synoptic patterns favoring the SA activity:

- Destabilization of the increasingly thicker snow cover (> 60 cm) during warm periods in January;

- Snow cover destabilization due to the combined effect caused by the very hot and rainy days during April;
- Cold periods with snowfall and strong winds during November.

Our dendrogeomorphic reconstructions contribute to a better understanding of the pattern of SA activity at the subregional scale. However, further tree-ring studies extended to multiple paths in other subregions of the Rodna Mountains and corroborated with the analysis of weather conditions would provide an improved knowledge regarding the SA regime and the conditions favorable to SA activity at the regional scale.

The avalanche winters reconstructed using a tree-ring approach can be further used to identify the synoptic controls on avalanche activity and inform hazard management decision-makers regarding the frequency and spatial extent of SAs in the affected areas. Our reconstructions can help the Administration of the Rodna Mountains National Park in their effort to implement appropriate avalanche hazard planning for safe tourism activities in the avalanche-prone areas.

Acknowledgements This work was supported by the Agence Universitaire de la Francophonie (AUF) and Institute of Atomic Physics (IFA) in Romania under Grant 09-AUF-ACTIVNEIGE "*Activité des avalanches de neige dans les Carpates Orientales Roumaines et Ukrainiennes.*" The two anonymous reviewers are acknowledged for their positive comments which improved the earlier version of the manuscript. We acknowledge the suggestions provided by Adina Croitoru and Oana-Alexandra Dumitru, which kindly accepted to check the English language of the manuscript text.

Author contributions All authors contributed to the study conception and design. Material preparation, data collection, and analysis were performed by all the authors. The first draft of the manuscript was written by Ionela Georgiana Gavrilă, Olimpiu Traian Pop, and Iulian Horea Holobâcă, and all authors commented on previous versions of the manuscript. All authors read and approved the final manuscript.

Declarations

Conflict of interest The authors report there is no competing interest to declare.

References

Boucher D, Filion L, Hétu B (2003) Reconstitution dendrochronologique et fréquence des grosses avalanches de neige dans un couloir subalpin du Mont Hog's Back, Gaspésie Centrale. Québec Géogr Phys Et Quatern 57(2–3):159–168

Bräker OU (2002) Measuring and data processing in tree–ring research – a methodological introduction. Dendrochronologia 20(1–3):203–216

Bryant CL, Butler DR, Vitek JD (1989) A statistical analysis of tree-ring dating in conjunction with snow avalanches: comparison of on-path versus off-path responses. Environ Geol Water Sci 14(1):53–59

Burrows CJ, Burrows VL (1976) Procedures for the study of snow avalanche chronology using growth layers of woody plants: Boulder, Colorado. Institute of Arctic and Alpine Research Occasional Paper 23, p 54

Butler DR, Malanson GP (1985) A history of high-magnitude snow-avalanches, Southern Glacier National Park, Montana, USA. Mt Res Dev 5:175–182

Butler DR, Sawyer CF (2008) Dendrogeomorphology and high-magnitude snow avalanches: a review and case study. Nat Hazard 8:303–309

Casteller A, Stöckli V, Villalba R, Mayer AC (2007) An evaluation of dendroecological indicators of snow avalanches in the Swiss Alps. Arct Antarct Alp Res 39:218–228

Casteller A, Christen M, Villalba R, Martínez H, Stöckli V, Leiva JC, Bartelt P (2008) Validating numerical simulations of snow avalanches using dendrochronology: the Cerro Ventana event in Northern Patagonia, Argentina. Nat Hazard 8:433–443

Casteller A, Villalba R, Araneo D, Stöckli V (2011) Reconstructing temporal patterns of snow avalanches at Lago del Desierto, southern Patagonian Andes. Cold Reg Sci Technol 67:68–78
Cheval S, Bîrsan MV, Dumitrescu A (2014) Climate variability in the Carpathian Mountains Region over 1961–2010. Global Planet Change 118:85–96
Chiroiu P, Stoffel M, Onaca A, Urdea P (2015) Testing dendrogeomorphic approaches and thresholds to reconstruct snow avalanche activity in the Făgăraș Mountains (Romanian Carpathians). Quat Geochronol 27:1–10
Corona C, Rovéra G, Lopez-Saez J, Stoffel M, Perfettini P (2010) Spatio-temporal reconstruction of snow avalanche activity using tree rings: Jean Jeanne avalanche talus, Massif de l'Oisans, France. CATENA 83:107–118
Decaulne A, Eggertsson Ó, Sæmundsson Þ (2012) A first dendrogeomorphologic approach of snow avalanche magnitude-frequency in Northern Iceland. Geomorphology 167–168:35–44
Decaulne A, Eggertsson A, Laute K, Beylich A (2013) Dendrogeomorphologic approach for snow-avalanche activity reconstruction in a maritime cold environment (upper Erdalen, Norway). Zeitschrift Für Geomorphol Suppl 2:55–68
Decaulne A, Eggertsson A, Laute K, Beylich A (2014) A 100-year extreme snow-avalanche record based on tree-ring researchin upper Bødalen, inner Nordfjord, western Norway. Geomorphology 218:3–15
Dragotă CS, Kucsicsa G (2011) Global climate change-related particularities in the Rodnei Mountains National Park. Carpathian J Earth Environ Sci 6(1):43–50
Dubé S, Filion L, Hétu B (2004) Tree-ring reconstruction of high-magnitude snow avalanches in the Northern Gaspé Peninsula, Québec, Canada. Arct Antarct Alp Res 36:555–564
Favillier A, Guillet S, Trappmann D, Morel P, Lopez-Saez J, Eckert N, Zenhäusern G, Peiry JL, Stoffel M, Corona C (2018) Spatio-temporal maps of past avalanche events derived from tree-ring analysis: a case study in the Zermatt valley (Valais, Switzerland). Cold Reg Sci Technol 154:9–22
Gądek B, Kaczka R, Rączkowska Z, Rojan E, Casteller A, Bebi P (2017) Snow avalanche activity in Żleb Żandarmerii in a time of climate change (Tatra Mts., Poland). CATENA 158:201–212
Germain D, Filion L, Hétu B (2005) Snow avalanche activity after fire and logging disturbances, Northern Gaspé Peninsula, Quebec, Canada. Can J Earth Sci 42:2103–2116
Germain D, Filion L, Hétu B (2009) Snow avalanche regime and climatic conditions in the Chic-Choc Range, Eastern Canada. Clim Change 92:141–167
Giacona F, Eckert N, Corona C, Mainieri R, Morin S, Stoffel M, Martin B, Naaim M (2021) Upslope migration of snow avalanches in a warming climate. Proc Natl Acad Sci USA 118(4):e2107306118. https://doi.org/10.1073/pnas.2107306118
Holmes RL (1983) Computer-assisted quality control in tree-ring dating and measuring. Tree-Ring Bull 43:69–78
Kogelnig-Mayer B, Stoffel M, Bollschweiler M, Hübl J, Rudolf-Miklau F (2011) Possibilities and limitations of dendrogeomorphic time-series reconstructions on sites influenced by debris flows and frequent snow avalanche activity. Arct Antarct Alp Res 43:649–658
Krause D, Křížek M (2018) Dating of recent avalanche events in the Eastern High Sudetes, Czech Republic. Quatern Int 470:166–175
Mainieri R, Favillier A, Lopez-Saez J, Eckert N, Zgheib T, Morel P, Saulnier M, Peiry JL, Stoffel M, Corona C (2020) Impacts of land-cover changes on snow avalanche activity in the French Alps. Anthropocene 30:10024. https://doi.org/10.1016/j.ancene.2020.100244
Mândrescu M, Evans IS, Cox NJ (2010) Climatic implications of cirque distribution in the Romanian Carpathians: palaeowind directions during glacial periods. J Quat Sci 25:875–888
McClung D, Schaerer P (2006) The avalanche handbook, 3rd edn. The Mountaineers Books, Seattle, USA
Micu DM, Dumitrescu A, Cheval S, Bîrsan MV (2016) Climate of the Romanian Carpathians. Variability and trends. Springer Cham, Germany
Muntán E, García C, Oller P, Martí G, García A, Gutiérrez E (2009) Reconstructing snow avalanches in the Southeastern Pyrenees. Nat Hazard 9:1599–1612
Peitzsch E, Hendrikx J, Stahle D, Pederson G, Birkeland K, Fagre D (2021) A regional spatiotemporal analysis of large magnitude snow avalanches using tree rings. Nat Hazard 21:533–557
Pop OT, Gavrilă IG, Roşian G, Meseşan F, Decaulne A, Holobâcă IH, Anghel T (2016) A century-long snow avalanche chronology reconstructed from tree-rings in Parang Mountains (Southern Carpathians, Romania). Quatern Int 415:430–440
Pop OT, Munteanu A, Flaviu M, Gavrilă IG, Timofte C, Holobâcă IH (2018) Tree-ring-based reconstruction of high-magnitude snow avalanches in Piatra Craiului Mountains (Southern Carpathians, Romania). Geogr Ann Ser B 100:99–115
Rayback SA (1998) A dendrogeomorphological analysis of snow avalanches in the Colorado Front Range, USA. Phys Geogr 19:502–515

Reardon BA, Pederson GT, Caruso CJ, Fagre DB (2008) Spatial reconstructions and comparisons of historic snow avalanche frequency and extent using tree rings in Glacier National Park, Montana, USA. Arct Antarct Alp Res 40:148–160

RINNTECH (2021) Technology for tree and wood analysis. Accessed December 11, 2021 http://www.rinntech.de/index-28703.html

Schweizer J, Jamieson JB, Schneebeli M (2003) Snow avalanche formation. Rev Geophys 41(4):2–25

Shroder JF (1978) Dendrogeomorphological analysis of mass-movement, Table Cliff Plateau, Utah. Quatern Res 9:168–185

Šilhán K, Stoffel M (2015) Impacts of age-dependent tree sensitivity and dating approaches on dendrogeomorphic time series of landslides. Geomorphology 236:34–43

Šilhán K, Tichavský R (2017) Snow-avalance and debris-flow activity in the High Tatras Mountains: new data from using dendrogeomorphic survey. Cold Reg Sci Technol 134:45–53

Šilhán K, Kluzová O, Tichavský R (2019) The on field differentiation of snow avalanche- and debris flow-induced scars in trees as a fundament for improving dendrogeomorphic sampling strategy (case study from the Great Cold Valley in High Tatra Mountains). Cold Reg Sci Technol 158:1–9

Stoffel M (2008) Dating past geomorphic processes with tangential rows of traumatic resin ducts. Dendrochronologia 26:53–60

Stoffel M, Bollschweiler M (2008) Tree-ring analysis in natural hazards research – an overview. Nat Hazard 8:187–202

Stoffel M, Corona C (2014) Dendroecological dating of geomorphic disturbance in trees. Tree-Ring Res 70(1):3–20

Stoffel M, Bollschweiler M, Hassler GR (2006) Differentiating past events on a cone influenced by debris-flow and snow avalanche activity - a dendrogeomorphological approach. Earth Surf Process Landforms 31(11):1424–1437

Stoffel M, Butler D, Corona C (2013) Mass movements and tree rings: a guide to dendrogeomorphic field sampling and dating. Geomorphology 200:106–120

Tank KAMG, Wijngaard JB, Können GP, Böhm R, Demarée G, Gocheva A, Mileta M et al (2002) Daily dataset of 20th-century surface air temperature and precipitation series for the European Climate Assessment. Int J Climatol 22:1441–1453

Tichavský R, Šilhán K (2016) The changing ability of Norway spruce (P. abies) to record hydro-geomorphic processes based on the age and diameter of the tree stem – a dendrogeomorphic approach. CATENA 147:469–480

Tichavský R, Šilhán K, Stoffel M (2017) Age-dependent sensitivity of trees disturbed by debris flows-implications for dendrogeomorphic reconstructions. Quat Geochronol 42:63–75

Todea C, Pop OT, Germain D (2020) Snow–avalanche history reconstructed with tree rings in Parâng Mountains (Southern Carpathians, Romania). Revista De Geomorfol 22:73–85

Tumajer J, Treml V (2015) Reconstruction ability of dendrochronology in dating avalanche events in the Giant Mountains, Czech Republic. Dendrochronologia 34:1–9

Urdea P, Reuther Anne U (2009) Some new data concerning the quaternary glaciation in the Romanian Carpathians. Geogr Pannon 13(2):41–52